



Distributed optical fiber vibration sensing using phase-generated carrier demodulation algorithm

Zhihua Yu^{1,2} · Qi Zhang^{1,2} · Mingyu Zhang^{1,2} · Haolong Dai^{1,2} · Jingjing Zhang^{1,2} · Li Liu^{1,2} · Lijun Zhang^{1,2} · Xing Jin^{1,2} · Gaifang Wang^{1,2} · Guang Qi^{1,2}

Received: 26 October 2017 / Accepted: 21 April 2018 / Published online: 27 April 2018
© Springer-Verlag GmbH Germany, part of Springer Nature 2018

Abstract

A novel optical fiber-distributed vibration-sensing system is proposed, which is based on self-interference of Rayleigh backscattering with phase-generated carrier (PGC) demodulation algorithm. Pulsed lights are sent into the sensing fiber and the Rayleigh backscattering light from a certain position along the sensing fiber would interfere through an unbalanced Michelson interferometry to generate the interference light. An improved PGC demodulation algorithm is carried out to recover the phase information of the interference signal, which carries the sensing information. Three vibration events were applied simultaneously to different positions over 2000 m sensing fiber and demodulated correctly. The spatial resolution is 10 m, and the noise level of the Φ -OTDR system we proposed is about 10^{-3} rad/ $\sqrt{\text{Hz}}$, and the signal-to-noise ratio is about 30.34 dB.

1 Introduction

Recently, distributed fiber-optic vibration sensors receive extensive investigation and play a significant role in the sensor panorama [1–3]. When external intrusion is applied on a certain part of the sensing fiber, some of the optical parameters, such as light intensity, phase, polarization state, or light frequency, will change. Compared with point and quasi-distributed, distributed fiber-optic vibration sensors have not only the advantages of general fiber sensors, but also can offer such advantages as light weight, large-scale monitoring, good concealment, excellent flexibility, high sensitivity, accurate location, etc [4–6].

Distributed optical fiber vibration measurements mainly include optical fiber interferometer sensors and optical backscattering based sensors. In general, interferometer sensors, such as Sagnac, Michelson [7, 8], and Mach–Zehnder [9], integrate a signal light and a reference light to acquire distributed information. Due to the differences between two correlated signals caused by noises or changes of polarization state, the spatial resolution of these interferometers is

not satisfied, since only one random event can be positioned. Another distinguished technique is the use of optical backscattering based sensors. Polarization optical time domain reflectometer (POTDR) has achieved 10 m spatial resolution in 1 km sensing range, while the detected frequency response is 5 kHz [10]. The limitation of POTDR is that they are incapable of determining the full vibration information, namely, the amplitude, frequency, and phase of the incident signal, which is a necessity for seismic imaging [11]. Measuring the full vibration information is a much harder technical challenge to overcome. A promising technique is phase sensitive optical time domain reflectometer (Φ -OTDR) using a narrow line-width laser, which has been demonstrated [12, 13].

In this paper, we proposed an optical fiber-distributed vibration-sensing system based on self-interference of Rayleigh backscattering with an improved phase-generated carrier (PGC) demodulation algorithm. This scheme differs from the previous schemes in that it combines with Φ -OTDR and Michelson interferometry (MI) and would have advantages both of them. Experiments on detection of multiple piezoelectric transducers show that our system can well describe multiple different vibration signals with a good signal-to-noise ratio (SNR). The vibration event information such as amplitude, frequency, and location can be directly obtained using an improved PGC demodulation algorithm. This novel vibration measurement scheme can be applied at

✉ Zhihua Yu
yuzhuhua@cug.edu.cn

¹ School of Automation, China University of Geosciences, Wuhan, Hubei, China

² Hubei key Laboratory of Advanced Control and Intelligent Automation for Complex Systems, Wuhan, Hubei, China

surface, seabed, or downhole for vibration measurements or distributed acoustic sensing (DAS).

2 Principle

2.1 Self-interferometer of Rayleigh backscattering based on Michelson interferometer

Normally, Φ -OTDR techniques, where the system is probed with narrow coherent light pulses with direct detection [14, 15], is used. Here, we add a Michelson interferometer (MI) to the receiving end of the Φ -OTDR. The basic principle of distributed fiber vibration sensing based on Φ -OTDR is detecting the phase change induced by the coherent Rayleigh scattering caused by multiple scattering centers within the injected pulse duration. With the introduce of an unbalanced MI, where the arm length difference is d , the Rayleigh scattering light from a certain position along the sensing fiber would interfere and generates interference light, whose phase carries the sensing information. The principle scheme of Φ -OTDR system with an unbalanced MI introduced at the receiving end is shown in Fig. 1.

The Rayleigh scattering is caused by scattering centers with random distribution along the sensing fiber, the electrical field of backscattered light of every scattering center has independent amplitude and phase, the sum of them constitutes the electrical field of backscattered Rayleigh light. Assuming that the scattering unit has i scattering centers and the polarization state between each scattering center is consistent, then, the electrical field of the scattering center from the position $L_i = i\Delta L$ can be written as

$$E_{L_i}(t) = E_0 P_i \exp(-\alpha L_i) \cdot \exp(-j2\beta L_i) \cdot a_i \exp[j\varphi_i(t)], \quad (1)$$

where E_0 is the electric field intensity of incident light, P_i has the relationship with polarization state, α is the optical power attenuation coefficient, β is the propagation constant, and α_i and φ_i are the reflectivity and phase of scattering unit.

As shown in Fig. 1, when $E_L(t)$ is injected into MI, one of the two paths is utilized as delay light and the optical path

difference is d , so the interference light intensity from the position L can be expressed as

$$\begin{aligned} E(t) &= E_L(t) + E_{L-d}(t) = E_0 P_n \exp(-\alpha L) \cdot \exp(-j2\beta L) \\ &\cdot a_i \exp[j\varphi_n(t)] + E_0 P_{nd} \exp(-\alpha(L+d)) \\ &\cdot \exp(-j2\beta(L+d)) \cdot a_i \exp[j\varphi_n(t)] \cdot \{\exp(j\beta d) \\ &\cdot \exp[j\varphi_{nd}(t) - j\varphi_n(t)]\} = M + N \cdot \exp(j\beta d + \Delta\varphi(t)). \end{aligned} \quad (2)$$

Here, we assume that $\Delta\varphi(t) = \varphi_{nd}(t) - \varphi_n(t)$ and the coefficients are simplified as M and N . The output power of interference light through the MI is

$$\begin{aligned} I(t) &= |E(t)|^2 = M^2 + N^2 + 2MN \cos[\beta d + \Delta\varphi(t)] \\ &= A + B \cos(\varphi(t)). \end{aligned} \quad (3)$$

When a PGC signal, whose frequency is ω_0 , modulates one arm of MI using a PZT, the phase of interference light adds a phase modulation term $m\Delta d \cos(\omega_0 t)$, where m is the modulation index and Δd is the maximum length difference variation of MI. We can assume $m\Delta d = C$, so the total phase of the interference light is $C \cos(\omega_0 t) + \varphi(t)$ and the output can be expressed:

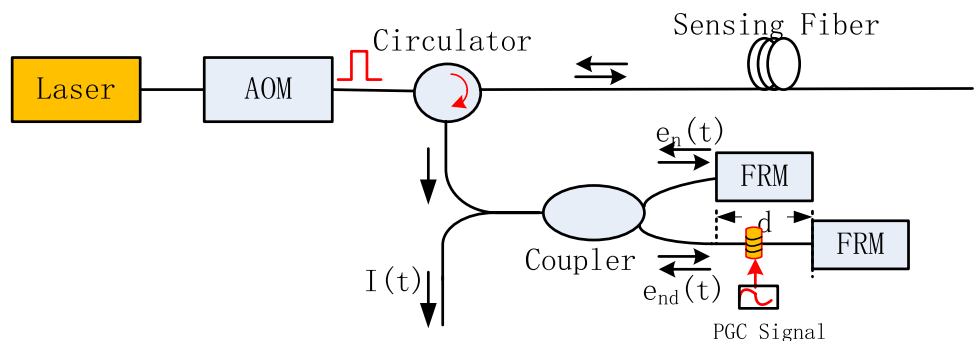
$$I(t) = A + B \cos(C \cos(\omega_0 t) + \varphi(t)). \quad (4)$$

The quantity $\varphi(t)$ denotes the phase difference between the backscattered waves from different scatterers with the half arm length d . Therefore, the interference term $I(t)$ is a function of $\varphi(t)$, which is related to the vibration response in the sensing fiber.

2.2 An improved PGC demodulation method

Phase generation carrier (PGC) modulation and demodulation technology is a kind of passive homodyne demodulation technology, which is widely used in demodulation systems for its high sensitivity, good linearity, and large dynamic range. Here, we propose an improved carrier demodulation algorithm to demodulate the intruder signal, aiming to reduce system memory consumption and lower minimum sampling frequency.

Fig. 1 Schematic diagram of the self-interferometer of Rayleigh backscattering based on Michelson Interferometer



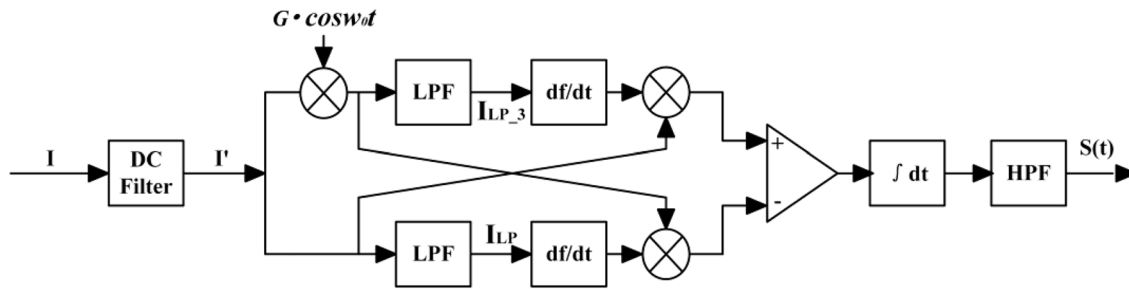


Fig. 2 Improved PGC demodulation scheme. \otimes , multiplier; *LPF*, low-pass filter; df/dt , derivative; \int , integrator; *HPF* high pass filter

The improved PGC demodulation algorithm block diagram is shown in Fig. 2. The interference signal I is filtered out by a DC filter, then one path is multiplied with $G \cos \omega_0 t$, and the other path directly goes through the low-pass filter. Finally, through the relevant processing with cross-differential and cross-multiply, we can achieve the demodulation signal $S(t)$.

Through the previous analysis, the interferometer output I can be expressed as

$$I = A + B \cdot \cos[C \cdot \cos \omega_0 t + \varphi(t)], \tag{5}$$

where $\varphi(t) = D \cos \omega_s t + \varphi_0(t)$, $D \cos \omega_s t$ is phase change induced by the tested signal, and $\varphi_0(t)$ is slow variation of the initial phase caused by environment and delay phase difference (βd).

According to the above formula (1), the interference signal after filtering the DC term is

$$I' = B \cdot \cos[C \cdot \cos \omega_0 t + \varphi(t)]. \tag{6}$$

Then, we can get

$$I_{LP_3} = -GBJ_1(C) \sin \varphi(t), \tag{7}$$

$$I_{LP} = BJ_0(C) \cos \varphi(t), \tag{8}$$

where $J_1(C)$ is a first order Bessel function.

Therefore, the final output $S(t)$ of the PGC which contains the tested signal $D \cos \omega_s t$ is

$$S(t) = GB^2 J_0(C) J_1(C) \cdot \varphi(t) = GB^2 J_0(C) J_1(C) D \cos \omega_s t, \tag{9}$$

where G is the fundamental amplitude.

According to Eq. (9), we can see that the final result of demodulation is related to $J_0(C)J_1(C)$ and the best value of C should be as small as possible, so that the value of $J_0(C)J_1(C)$ can close to a constant. Therefore, we can obtain the best phase modulation value of C is 1.1, in which $J_0(C) = 0.7196$, $J_1(C) = 0.4709$, $J_2(C) = 0.1366$, $J_3(C) = 0.0257$, $J_4(C) = 0.0036\dots$ When the order k increases, the value of $J_k(C)$ gradually decreases sharply. According to the phase modulation signal engineering principles, when the signal amplitude is less than 10%, it could be

neglected. Since $J_4(C)$ is already much smaller than 1, the spectrum of the interference signal will be mainly concentrated in $3\omega_0 + \omega_d$, where ω_d is the spectrum of the upper frequency or lower frequency on both sides of the carrier. Then, according to Nyquist sampling theorem, the minimum sampling frequency required for the lossless recovery signal must satisfy $\omega_T \geq (3\omega_0 + \omega_d)$. Thus, the highest demodulated frequency is $\omega_0 + \omega_d$, and also, we need promise that $\omega_0 + \omega_d$ could not be mixed with $3\omega_0 + \omega_d$. In other words, the minimum sampling frequency must satisfy $\omega_T - (3\omega_0 + \omega_d) > \omega_0 + \omega_d$, that is $\omega_T \geq 4\omega_0 + 2\omega_d$.

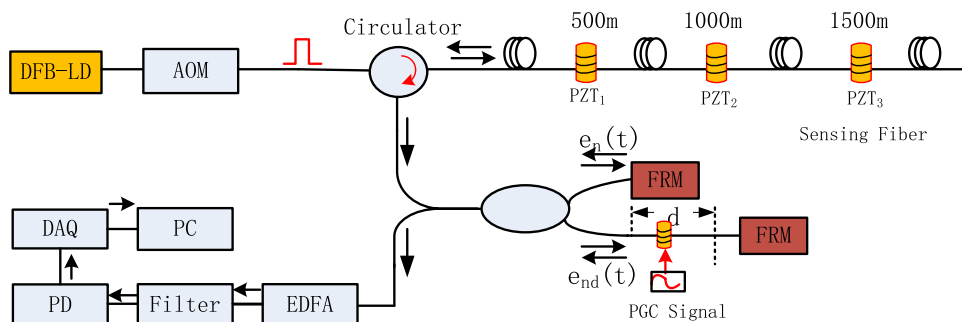
While in traditional PGC-DCM algorithm, the best C value is 2.37, so the spectrum of the interference signal is mainly concentrated in $4\omega_0 + \omega_d$, and the minimum sampling frequency must satisfy $\omega_T \geq 6\omega_0 + 2\omega_d$. Therefore, comparing traditional PGC-DCM algorithm, the minimum sampling frequency in our improved PGC demodulation method reduces by about one-third, and the memory consumption will reduce greatly.

3 Experiments and results

3.1 Experiment configuration of optical fiber-distributed vibration-sensing system

The experimental setup of our proposed Φ -OTDR based on Michelson interferometer is shown in Fig. 3. The light source is a narrow line-width laser with maximum output power of 30 mW and linewidth of 5 kHz. The CW light with a wavelength of 1550.12 nm is injected into an acoustic-optic modulator (AOM) to generate the pulses, whose width is 100 ns and the repetition rate R is fixed at 20 kHz. The maximum detection length is governed by the optical loss along the sensing fiber and the number of sampling points which can be processed in the system. The time interval among the pulses should be larger than the round trip time in that the pulses travel in the detection fiber to keep only one pulse inside the detection fiber. For

Fig. 3 Experiment setup of distributed vibration-sensing system



the 20 kHz repetition rate, the detection range is around 5 km which is determined by $L < c/2fn_f$. The detection frequency range is also related to the repetition rate f . In our case, the highest detection frequency is no more than 20 kHz theoretically.

Taking 2000 m length of fiber (Corning SMF-28e), for example, the experiment proves the above scheme. The modulated pulses are amplified by Erbium-doped fiber amplifier (EDFA) to get a suitable peak power at 1w, the output of EDFA is filtered by a narrow-band filter with a linewidth of 0.03 nm to remove spontaneous emission. Then, the amplified pulses are launched into a single-mode detection fiber by a circulator. When the sensing fiber detects a vibration, the phase information of Rayleigh backscattered light changes. Rayleigh backscattered light is then split into two paths by a 3 dB fiber coupler (50:50). One path is utilized as delay light, while the other path is modulated by Phase Modulator with 60 kHz frequency, and the optical path imbalance is half-spatial resolution of 20 m according to pulsewidth (W) of 100 ns. The two paths of backscattering light would interfere at the output of MI and generate interference signal. The phase of the interference signal carries sensing information, like vibration events. A high-sensitivity PD with 50 M bandwidth is used to detect the coherent back Rayleigh scattered light traces. The output of PD is sampled by DAQ simultaneously with 200 MS/s sampling rate. The acquired signals on PD consist of a train of backscattered traces. The length of each trace is proportional to the length of the sensing fiber. The sequence of traces is rearranged to provide the backscattered traces and allows the output at a particular position to be determined as a function of time. The improved PGC demodulation scheme is implemented digitally for one particular position along the fiber. A fast Fourier transform is performed to identify the frequency components of any phase perturbation occurring within the gauge length of this point.

In our current system setup, the path difference of MI is 10 m with interrogating pulse width of 100 ns, providing a spatial resolution of 10 m. This value is determined by the fiber delay between two arms of MI. The spatial resolution

can be improved by reducing the pulse duration and the path difference of MI simultaneously.

3.2 Experiment results

To evaluate the monitoring performance of multiple vibration sources, three piezoelectric transducer (PZT) cylinders with 10 m single-mode fiber wound are put at 500, 1000, and 1500 m over 2000 m detection fiber as the vibration sources. The PZTs ($s = 1, 2, 3$) are driven by a function generator and the fiber is fixed on the surface of the PZTs cylinder by instant glue in order that the vibration of the PZTs can be transmitted to the fiber. We set the function generator to output a sine wave with the frequency of 1000 Hz and the amplitude of 1 V. The global demodulation result of the 2000 m detection fiber is given in Fig. 4a. We can see clearly that there exist three vibrations located at about 500, 1000, and 1500 m.

In addition, we set the three function generators to output sine waves with the same frequency of 500 Hz as the former, but their amplitudes are different, whose amplitudes were 0.5, 1, and 1.5 rad, respectively. The global demodulation results are shown in Fig. 4b. We can see that three vibration signals were detected: the first demodulated peak located at about 500 m with the amplitude of 0.5 rad, the second one located at about 1000 m with the amplitude of 1 rad, and the last one located at about 1500 m with the amplitude of 1.5 rad. Except for these three sine-like signals, there are no other vibration in the global demodulation result, which indicates no influence of other backscatters of the whole sensing fiber during the demodulation process. Through these experiments, this system could detect locations and amplitudes of multiple vibration signals successfully.

To fully verify the system distributed characteristics, we analyzed the vibration waveforms and frequency spectral at 1000 m via fast Fourier transform (FFT) using the above-mentioned PGC demodulation, as shown in Fig. 2. The demodulated 500 Hz signal given by our system fits very well with its original PZT source, which has the amplitude A_{1V} of about -2.06 dB [$= 20 \log_{10}(A_{\text{signal}})$, 0.788 rad], as shown in Fig. 5. It has almost the same spectral properties,

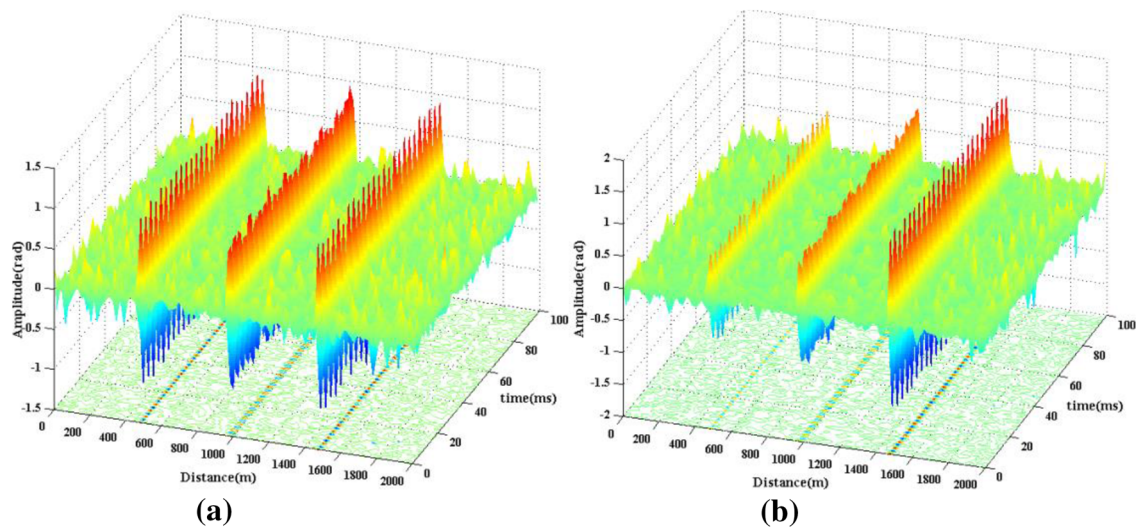


Fig. 4 Demodulation result of **a** three vibration events with the amplitude of 1 V with different frequency and locations; **b** three vibration events with the frequency of 500 Hz with different amplitudes and locations

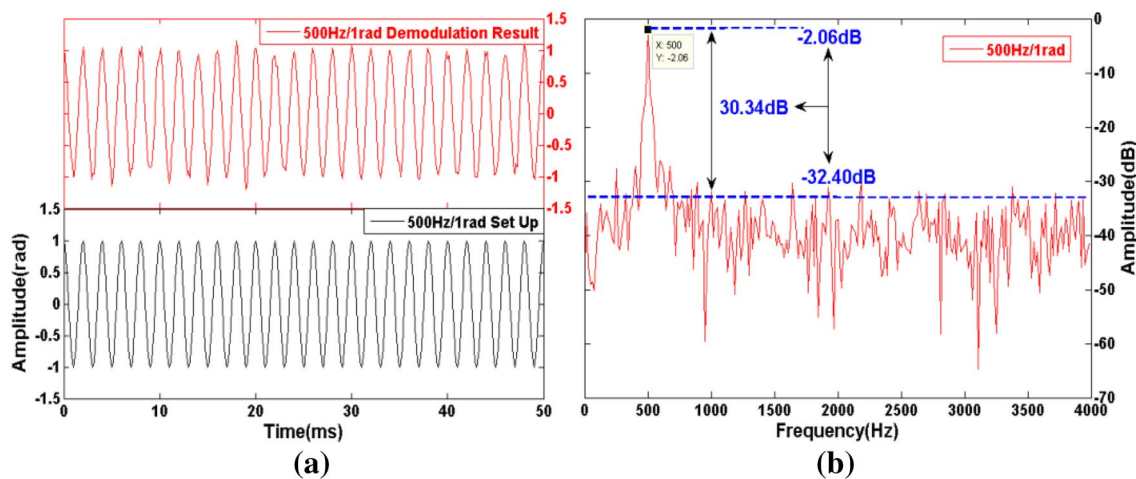


Fig. 5 Demodulation result of **a** time responses of the original PZT source and demodulation result of 500 Hz with 1 V; **b** frequency responses of the demodulation result of 500 Hz with 1 V

such as the low frequency component, as the PZT source. The background noise of the demodulated signal is about -32.40 dB ($10^{-3}\text{ rad}/\sqrt{\text{Hz}}[=0.024\text{ rad}/\sqrt{500\text{ Hz}}]$), so that the SNR [$=20\log_{10}(A_{1V}/A_{\text{noise}})$] is 30.34 dB. The result indicates that our Φ -OTDR interferometer system can fully demodulate frequency and spectral properties of the PZT source with a good SNR.

Figure 6a, b gives the waveforms of different frequency vibration sources in 1V. The frequency of the 500 Hz demodulated signal at 500 m is slightly increased to -2.041 dB (0.7906 rad), the 1000 Hz demodulated signal at 500 m is slightly increased to -2.167 dB (0.7792 rad), and the 1500 Hz demodulated signal at 500 m is slightly

increased to -2.173 dB (0.7787 rad). We can see that different frequencies target signals with the same amplitude have no obvious influences and they could be successfully demodulated. Through the frequency domain demodulation, we obtained the SNRs are significantly greater than 30 dB.

Figure 7a, b shows the waveforms of different amplitudes vibration sources in 500 Hz. The amplitude of the 1V demodulated signal at 1000 m is slightly increased to -2.025 dB (0.7920 rad), the amplitude of the 1.5 V demodulated signal at 1000 m is about 1.415 dB (1.1769 rad), and the amplitude of the 2V demodulated signal at 1000 m is about 3.892 dB (1.5653 rad). The amplitude rate A_{2V}/A_{1V}

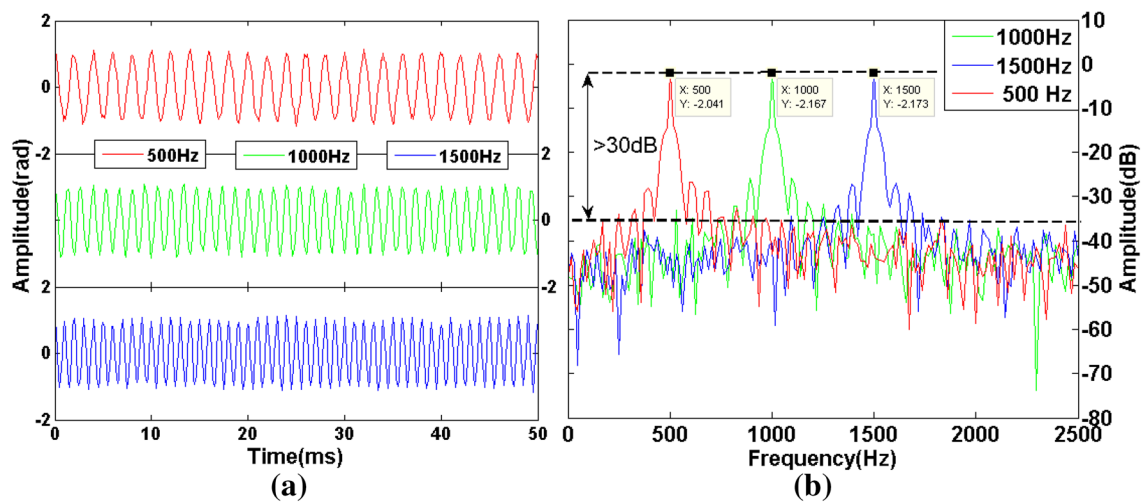


Fig. 6 a, b Time and frequency responses of the demodulation result of 500, 1000, and 1500 Hz with 1V

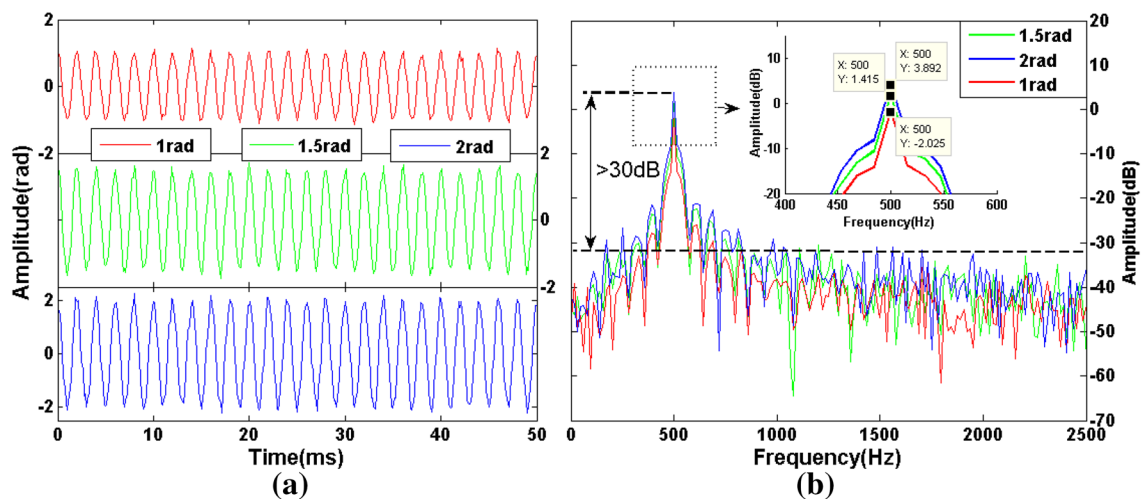


Fig. 7 a, b Time and frequency responses of the original PZT source and demodulation result of 500 Hz with 1, 1.5, and 2 V

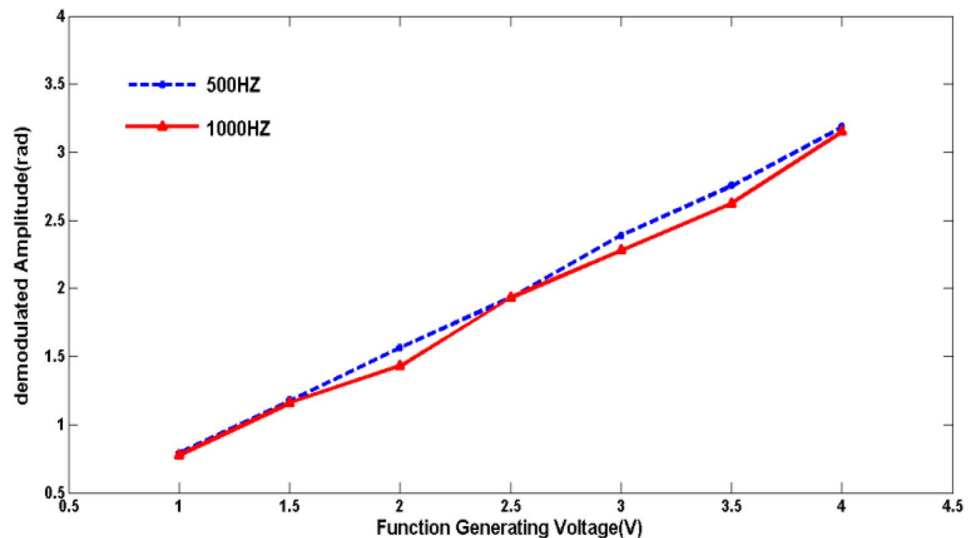
(1.5653/0.7920) is about 1.9764 dB, nearly twice between the 2 and 1 V signal amplitudes.

Moreover, we also set the vibration source in 1000 Hz with different voltages to testify the demodulating accuracy of the amplitude proportions along with the same situation. The generating amplitudes are set from 1 to 4 V. The demodulation results are shown in Fig. 8. In the blue curve of 500 Hz ($A_{2.5V}=1.9316$ rad, $A_{3V}=2.3869$ rad, $A_{3.5V}=2.7532$ rad, $A_{4V}=3.1845$ rad @ 500 Hz), the amplitude of 4 V demodulated signal (A_{4V}) is almost eight times larger than that of the 1 V demodulated signal (A_{1V}). In addition, although the 1000 Hz demodulated amplitudes are different slightly from those of 500 Hz at the same

generating voltage because of the different frequency response of our PZTs, they still exhibit a nearly linear relation ($A_{1V}=0.7724$ rad, $A_{1.5V}=1.1577$ rad, $A_{2V}=1.4293$ rad, $A_{2.5V}=1.9317$ rad, $A_{3V}=2.2785$ rad, $A_{3.5V}=2.6263$ rad, $A_{4V}=3.1513$ rad @ 1000 Hz). Under the real circumstance, the phase change would be the same at different frequencies when the acoustic pressure is constant.

Through the above experiments, the distributed and positioning characteristics of the system have been verified. The proposed Φ -OTDR interferometer system can well demodulate the amplitude, frequency, and phase of multiple vibration signals simultaneously. The background noise is around -32 dB and the SNR is about 30.34 dB. Further experiments will be done using water tank and

Fig. 8 Demodulated amplitude information with different function generating voltages at 500 and 1000 Hz, respectively



underwater speaker to detect real sound waves with larger frequency range.

4 Conclusion

In this paper, a novel Φ -OTDR system is proposed based on self-interference of Rayleigh backscattering with an improved phase-generated carrier (PGC) demodulation algorithm to realize distributed fiber sensing. Pulsed lights are sent into the sensing fiber and the Rayleigh scattering light from a certain position along the sensing fiber would interfere through an unbalanced MI to generate the interference light. A new PGC demodulation algorithm is carried out to recover the phase information of the interference signal, which carries the sensing information. Multiple vibration events are applied to different positions of the sensing fiber and we realize to demodulate it correctly. The sensing length and the spatial resolution of the Φ -OTDR system are 2000 and 10 m and the noise level of the Φ -OTDR we proposed is about $10^{-3}\text{rad}/\sqrt{\text{Hz}}$, and an SNR about 30.34 dB is achieved.

Acknowledgements The authors would like to acknowledge the support of National Natural Science Foundation of China (NSFC) under Grant 61205089 and 61604135, Projects of Wuhan Science and Technology Program under Grant 2017010201010130.

References

1. Y. Wang, B. Jin, Y. Wang, D. Wang, X. Liu, Q. Bai, Real-time distributed vibration monitoring system using Φ -OTDR. *IEEE Sens. J.* **17**(5), 1333–1341 (2017)
2. X. Bao, L. Chen, Rechen progress in distributed fiber optic sensors. *Sensors* **12**, 8601–8639 (2012)
3. Y. Wang, X. Liu, B. Jin, X. Song, D. Wang, Q. Bai, Optical fiber vibration sensor using chaotic laser. *IEEE Photon. Technol. Lett.* **29**(16), 1336–1339 (2017)
4. X. Liu, B. Jin, Q. Bai, Y. Wang, Y. Wang, Distributed Fiber-optic sensors for vibration detection. *Sensors* **16**, 1164 (2016)
5. M.G. Tanner, S.D. Dyer, B. Baek, R.H. Hadfield, S.W. Nam, High-resolution single-mode fiber-optic distributed Raman sensor for absolute temperature measurement using superconducting nanowire single-photon detectors. *Appl. Phys. Lett.* **99**(20), 201110 (2011)
6. Y. Dong, H. Zhang, L. Chen, X. Bao, 2 cm spatial-resolution and 2 km range Brillouin optical fiber sensor using a transient differential pulse pair. *Appl. Opt.* vol. **51**(9), 1229–1235 (2012)
7. G. Bolognini, J. Park, M.A. Soto, N. Park, F.D. Pasquale, Analysis of distributed temperature sensing based on Raman scattering using OTDR coding and discrete Raman amplification. *Meas. Sci. Technol.* **18**(18), 3211–3218 (2007)
8. S.E. Watkins, Smart bridges with fiber-optic sensors. *IEEE Instrum. Meas. Mag.* **6**(2), 25–30 (2003)
9. X. Hong, J. Wu, C. Zuo, F. Liu, H. Guo, K. Xu, Dual Michelson interferometers for distributed vibration detection. *Appl. Opt.* **50**(22), 4333–4338 (2011)
10. Q. Sun, D. Liu, J. Wang, H. Liu, Distributed fiber-optic vibration sensor using a ring Mach–Zehnder interferometer. *Opt. Commun.* vol. **281**, 1538–1544 (2008)
11. T.M. Daley, B.M. Freifeld, J.A. Franklin, S. Dou, R. Pevzner, V. Shulakova, S. Kashikar, D.E. Miller, J. Goetz, J. Hennings, S. Lueth, Field testing of fiber-optic distributed acoustic sensing (DAS) for subsurface seismic monitoring. *Lead. Edge* **32**, 936–942 (2013)
12. Y.L. Lu, T. Zhu, L.A. Chen, X.Y. Bao, Distributed vibration sensor based on coherent detection of phase-OTDR. *J. Lightwave Technol.* **28**, 3243–3249 (2010)
13. X. Hong, H. Guo, J. Wu, K. Xu, Y. Zuo, Y. Li, J. Lin, An intrusion detection sensor based on coherent optical time domain reflector. *Microw. Opt. Technol. Lett.* **52**(12), 2746–2748 (2010)
14. A. Masoudi, M. Belal, T.P. Newson, A distributed optical fibre dynamic strain sensor based on phase-OTDR. *Meas. Sci. Technol.* **24**(8), 085204 (2013)
15. Y. Muanenda, C.J. Oton, S. Faralli, F.D. Pasquale, A cost-effective distributed acoustic sensor using a commercial off-the-shelf DFB laser and direct detection phase-OTDR. *IEEE Photon. J.* **8**(1), 6800210 (2016)